Hydrodynamic Behaviour of Compacted Granite Sawdust from the Dimension Stone Industry of Pontevedra (Spain): Experimental and Modelling

by

Ismael Falcon-Suarez[1]

Ricardo Juncosa-Rivera[2]

Phil Vardon[3]

Dieter Rammlmair[4]

Thomas Gunter[4]

Ulla Noell[4]

&

Jordi Delgado-Martin[2]

(1) National Oceanography Centre, University of Southampton Waterfront Campus. European Way, SO14 3ZH, Southampton, United Kingdom.

(2) Civil Engineering School. University of A Coruña. Campus de Elviña s/n. 15192 A Coruña. Spain

(3) Geo-Engineering Section, Delft. University of Technology, PO-box 5048, 2600 GA Delft. The Netherlands

(4) Federal Institute for Geosciences and Natural Resources (BGR), Stilleweg 2, 30655 Hannover. Germany

*Corresponding author: National Oceanography Centre, University of Southampton Waterfront Campus. European Way, SO14 3ZH, Southampton.

Phone: +44 (0)23 8059 6666   Office: 786/15   e_mail: isfalc@noc.ac.uk

Abstract

Two large-scale column experiments have been performed to test the hydrodynamic behaviour of unsaturated, compacted granite sawdust - a material produced during the dressing of dimension stone in Pontevedra (Spain). One of the columns was equipped with psychrometers and capacity probes while, in the other, a radial array of 80 electrodes made possible a time-dependent 3D electrical resistivity survey. All these devices allowed investigating and modelling the progressive saturation of the material. The study includes a straightforward methodology developed to calibrate the resistivity signals based on standard Proctor-compacted specimens. The progressive saturation of the granite sawdust reveals different stages: initially, an uneven advance of the saturation front (fingering) occurs; later on, this feature vanishes and is replaced by a more regular advance of the saturation front. Numerical analysis of the results shows that the yield capacity of the granite sawdust is ~0.39 m^3 m^{-3} and a saturated hydraulic conductivity ~$2 \cdot 10^{-6}$ m s^{-1}. The last value, which corresponds to the specific standard Proctor compaction, is not sufficient to support the use of granite sawdust for compacted-single-layer capping structures. Nonetheless, increased compaction efforts or improved design criteria (multilayer systems or capillary barriers) can keep bearing when considering granite sawdust for this purpose.

Key words:

Sustainable waste management, sanitary landfills, unsaturated soil behaviour, hydraulic conductivity, yield capacity, water fingering.

1 Introduction

The modern mining industry faces a significant environmental challenge related with the sustainable management and safe disposal of their processing wastes. Dimension stone industry is widespread worldwide and major producers concentrate rock extraction and processing in relatively reduced areas. This is the case in Pontevedra, Galicia (NW Spain) were only the granite industry generates ~2.2×10^5 tons of rock dust (granite sawdust) on a yearly basis (Barrientos et al., 2010).

The use of waste and by-products from mining and industrial activities (e.g. fly ash, dewatered sludge, quarry fines, mine tailings, etc.) in geotechnical engineering projects constitute a sustainable waste management approach (e.g. Borghetti et al. 2009; Carro et al. 2008; Falcon 2011; Fraser and McBride 2000; ICAR 2000; Navarro et al. 2008). However, this requires suitable studies of the material properties so that the considered by-product can be appropriately applied to solve engineering problems. In the case of sealing barriers specific restrictions apply according to Directive 1999/31/EC, where it is ruled that the sealing and capping layers in a landfills must comprise a mineral layer with combined properties of hydraulic conductivity and thickness that ensure the protection of soil, surface water and groundwater. To this respect, the requirement for the lining varies depending on the type of waste to be stored.

Based on different preliminary works (Vázquez 2005; Vázquez et al. 2007; Navarro et al. 2008; Carro et al. 2008; Barrientos et al. 2010; Falcon-Suarez 2011) the inert nature and small grain size of granite sawdust make it amenable of use in compacted sealing barriers provided that sufficient performance is attained. This performance is typically assessed in most engineering practice codes based on compacted thickness, hydraulic conductivity, geotechnical properties (plasticity and fines content) and waste compatibility issues (eg. Daniel and Koerner, 1993). Granite sawdust is made of fine grained, low plasticity natural inert minerals consisting of silty and clay size grains of granite particles with additional mineral components derived from the abrasive materials used in the workshops. Hence, the key point for its application as liner would be its hydrodynamic behavior.

The assessment of hydraulic conductivity in compacted clay materials is an standard practice in geotechnical laboratories (eg. ASTM D5856-15). However, it is well known that laboratory results often differ from in-situ behavior. For instace, Shackelford and Javed (1991) have pointed that the in-situ permeability of compacted clay soils can be as much as two to three orders of magnitude higher than the permeability values predicted by laboratory tests so that they suggest the convenience of performing big size (or large scale) permeability determinations in order to get more realistic estimates of this critical parameter. Keeping that in mind, in the present study we have performed a detailed assessment of the hydrodynamic behaviour of compacted, unsaturated granite sawdust specimens emplaced within PVC columns as they were progressively saturated and monitored with a variety of sensors to record the evolution of the corresponding moisture content. The monitoring survey has been also employed to model the unsaturated/saturated behaviour of the tested material.

In addition to material performance assessment, our study is also aimed at providing fundamental knowledge on the processes governing water transfer through a compacted fines barrier, to better understand the engineering limits of the studied material and to point towards acceptable technical solutions for the use of granite sawdust as liner.

2 Materials and Methods

2.1 Granite fines

Granite sawdust or granite fines (hereafter also called GF) is a granular material dominated by a silt-size fraction (10-15% clay; 70-75% silt; 10-15% fine sand), with low plasticity (class ML of the USCS classification scheme) and relatively small specific surface area (i.e., BET, 6 to 10 $m^2 g^{-1}$). The material includes quartz, feldspars (microcline, plagioclase) and phyllosilicates (biotite, muscovite, chlorite, etc.) among its mineralogical constituents, plus minor amounts of other minerals associated with the manufacturing processes in the workshops (mainly calcite and steel grit; 3 and 16 wt.%, respectively). Neglecting the origin, because of its small grain size and the type of infiltration tests used in this study, GF will be also referred to as soil within the text.

2.2 Experimental columns: assembly and initial test conditions

The experiments were conducted in two plastic columns (nominal capacity ~0.05 m^3 each), specifically designed to monitor the water flow through the soil during controlled flooding tests. The two columns were set up with different sensor configurations: column 1 (COL-1) used invasive sensors (capacitance probes and psychrometers); column 2 (COL-2) used non-invasive remote sensing of electrical conductivity (ring electrodes) to monitor changes in soil moisture content.

COL-1 was a 2 cm wall thickness acrylic column (0.5 m length; 0.35 m ID) closed at the bottom with two drains, and fitted with lateral ports to insert up to 12 sensors at different heights (Fig. 2a and Fig. 2b). The column was instrumented with four soil moisture sensors (ECHO EC-5) and eight psychrometers (PCT-55-15-SF Wescor Inc.) for measuring humidity variations along the column. Sensors were approximately located along the same axial plane. The bottom of the column was designed with a 2 cm high spacer-annulus (ID 27 cm, OD 31 cm) able to separate central leachates from those generated by preferential pathways at the interface between the column wall and the soil specimen. The column was filled with gravel up to the spacer height (2 cm) to prevent the occlusion of the pipework caused by fines migration and deposition. Above the gravel, eight layers of granite fines were stepwise poured and compacted with the aid of a modified Proctor hammer (ASTM-D1557 2009), on the basis of 75 hits per layer. Once compacted, each layer was sampled to obtain the initial properties shown in Table 1: water content was determined from oven-drying, while porosity and the remaining derived parameters were computed knowing the volume of a given layer (according to the layer height and the column diameter), using the density of solid particles reported by Barrientos et al. (2010). An extended formulation of the calculated parameters can be found in Falcon (2011).

COL-2 was a PVC tube (1.5 cm wall thickness; 0.75 m length; 0.3 m ID) perforated to insert 2 cm length electrodes distributed in five rings holding 16 units each (22.5º separation; Fig. 3a). The electrodes were connected to a SIPLab (Spectral Induced Polarization, Radic Research, Berlin) - a tool designed to measure resistivity in sediments and rocks. Likewise in COL-1, the bottom of the COL-2 column was also equipped with a spacer-annulus and filled with gravel up to the spacer height. A 35 cm thick layer of coarse sand was then used to fill the space between rings one and two. Sand was chosen to replace the GF in this region to avoid interpolation of moisture measurements that would be unrepresentative of the soil behaviour. Consequently, the study focused on the upper 25 cm of the column, where four rings of electrodes were located. Above the sand layer, four GF beds were poured above the sand, each compacted and sampled as described above for COL-1 (see initial conditions in Table 1).

The interpretation of resistivity measurements with SIPLab was based on the software BERT (Günther and Rücker 2013) which has been optimized for multielectrode array measurements either in the complex frequency domain or for direct-current. In our experiments, a direct current configuration (dipole-dipole; Seidel and Lange 2007) was adopted. That made possible the execution of up to 320 sequential measurements. One single cycle of measurement and processing lasted approximately 1 hour, which turns out to have a significant importance in terms of data interpretation. This is because the data from COL-2 is unable to fully describe the flow evolution, since each cycle represents resistivity values at different times. The electrical resistivity survey results in a 3D mesh of 8505 tetrahedral elements (Fig. 3b) which has been post processed with the aid of the software ParaView 3.8.0-RC1.

The GF used in both tests came directly from selected workshops located in Pontevedra, Spain and they had an initial water content of ~38 wt.%. To reduce the original moisture content, the material was primarily dehydrated (oven-drying, COL-1; lyophilisation, COL-2), and then partially rehydrated in a controlled manner. Since either inter- or intra-layer capillary effects might occur, particularly in the interfaces gravel-GF and sand-GF, the procedure adopted during specimen assembly was aimed at ensuring hydrodynamic equilibrium between layers, according to the following procedure. Firstly, both the gravel and sand were slightly hydrated (~0.3 of GF wt.%); secondly, the first layer of GF was compacted and covered with plastic sheeting (i.e., to minimize evaporation) for one day; thirdly, the layer of GF was sampled to gravimetrically determine its water content; finally, the remaining layers were hydrated according to the water/soil ratio determined for the first GF layer. Likewise, after being compacted, each subsequent layer was covered with plastic sheeting and sampled after about eight hours. Table 1 shows the results of the sampling, which represent the initial conditions of the tests.

2.3 Sensors calibration

Moisture influences the electrical response of a porous medium. When considering soils or rocks, the influence varies from one medium to another because the transmission of electrical current depends on the nature of the porous network (i.e., a combined effect of porosity, tortuosity and cementation of grains). Hence, determining the moisture of a soil through the electrical response requires calibration.

Separate calibrations were performed for the EC-5 soil moisture sensors and the electrode sensor arrays, since the way they detect the electrical response is different: while capacitance probes are based on induced polarization electrodes use direct current. Therefore, in COL-1, EC-5 sensors measure volumetric water content through the dielectric constant of the soil using capacitance technology (Campbell et al. 2005; Kelleners et al. 2004a; Kelleners et al. 2004b), which derives moisture content from changes in the permittivity of the porous medium; in COL-2, electrodes reciprocally act as transmitters of direct current and receptors of the electrical signal attenuated after travelling through the soil.

Calibration required soil specimens of well-known properties. Therefore, in the present study were performed standard Proctor tests (ASTM-D698, 2007) varying the water to soil ratio to cover the whole range of soil saturation: 34 and 28 Standard Proctor tests were used to calibrate capacitance sensors and electrodes, respectively. For each specimen, bulk density was calculated from the volume of the standard Proctor cell, while water content was gravimetrically determined; porosity and derived parameters were computed afterwards as referred earlier.

Soil moisture data from EC-5 were obtained by inserting the sensor in the soil specimen. For the measurement of the electrical response, the adopted protocol was as follow: first, the compacted Proctor specimen was transferred to an acrylic chamber of Proctor size (Fig. 4), and closed at both ends with wooden end-caps; second, four electrodes were inserted along the axis of the specimen through holes drilled in the acrylic cylinder; third, the electrodes were connected to SIPLab (at conditions of ±10V and ±10mA) to determine the bulk electrical resistivity of the sample, using a Wenner configuration (Seidel and Lange 2007).

Experimental data from the capacitance sensors were fitted with a third-order polynomial (Fig. 5) following the observations of Topp et al. (1980). Direct current measurements were corrected using the well-known Archie's relationship (Archie, 1942) which equates the porous medium bulk electrical conductivity (σ_b) with porosity (ϕ), degree of saturation (S_w), and the electrical conductivity of the pore fluid (σ_w):

$$\sigma_b = \frac{\phi^m S_w^n \sigma_w}{a} \qquad (1)$$

In the previous Eq. 1, m and n are cementation and saturation exponents, respectively, and *a* is the tortuosity factor. To determine σ_w, pore water was extracted from the Proctor specimens of highest water content using soil moisture pore water samplers (SMS) Rhizon (Falcon-Suarez et al. 2014; Seeberg-Elverfeldt et al. 2005). The electrical conductivity of extracted water (σ_w) was determined with standard benchtop conductivity meter, obtaining a mean value ~0.28 S m^{-1}. Then, the experimental parameters were adjusted by n=2.18, m=1.17, and a=0.92 (Fig. 6).

Thermocouple psychrometers measure air pressure, which is related to the relative humidity according to the Kelvin's equation (Vázquez, 2005; Falcon-Suarez, 2011). The psychrometers used in COL-1 were limited to the suction range of 8 to 0.05 MPa (±0.03 MPa) according to the technical specifications reported by the manufacturer (Wescor Inc.), who also provided calibration certificates. Therefore, no further calibrations were undertaken.

2.4 Test execution and data processing

The tests were developed simulating prescribed conditions of hydration from the top of the columns. Furthermore, evaporation (E) was also considered to calculate the water balance (BH). E was measured in an evaporation tank located in the laboratory, in the case of COL-1; for COL-2, E was assessed from the change in weight observed in a smaller column, similar to those used by Redwan and Rammlmair (2010) and Falcon-Suarez et al. (2014). This auxiliary column was filled with GF under similar moisture content and compaction conditions to those of COL-2, and also subjected to the same hydration process. Knowing the water poured (WP) and the volume of leachates (L) at the bottom, the water balance was determined by the expression $BH=WP-E-L$. This allowed the average saturation state of the porous media to be calculated based on the variation from its initial moisture content.

Watering was executed with the aid of nebulizers in order to minimize any erosive effect related to water impacting on the soil. During the test carried out in COL-1, the water infiltration was monitored by the EC-5 probes and psychrometers at frequencies of 0.033 and 0.017 Hz, respectively. In the case of the EC-5 sensors, the raw data were processed to correct the values according to the calibration function defined for granite fines (Fig. 5). Additionally, once leachates were observed, a last hydration step was purposely undertaken to flood the column. The aim was twofold: to observe the evolution of sensor reading under the highest moisture conditions, and to compute the mean hydraulic conductivity (K_0) by the constant head method.

In COL-2, the recorded resistivity data were inverted to obtain the bulk electrical conductivity of the soil (σ_b), and then transformed into degree of saturation by Archie's law using the experimental parameters for GF previously estimated and the electrical conductivity of the pore water (σ_w). To determine σ_w, at the end of the test pore water was extracted by inserting SMS Rhizon sensors using the 5 cm depth spaced electrode ports. A linear correlation with depth was determined (r^2=0.99) for electrical conductivity and this relationship was later used to compute S_w; the average value of σ_w along the column was ~0.18 S m^{-1}.

2.5 Infiltration flow modelling

The COMPASS code (COde for Modelling PArtly Saturated Soil, Thomas et al. 2012; Thomas and He 1997; Thomas and He 1998) was used to model the results of the experiment. COMPASS is a finite element code that allows simulation of soil behaviours using coupled multiphysical processes (i.e., unsaturated flow, heat and solute transport, and different mechanical phenomena). The software GID is a graphic interface coupled with COMPASS for pre- and post-processing data and visualization. It allowed the definition of the geometry of the problem (2D model); implementing the characteristics of the different layers, boundary conditions, the algorithms applied (Table 2) and temporal hydration curves; building the finite elements grid; calculating from COMPASS; and visualizing and editing results.

Only COL-1 was considered for modelling. A 2D grid of 5600 quadratic elements (5751 nodes) was used to simulate the central section of the column (0.35 m diameter; 0.38 m height). Initial conditions and geometry were defined according to the information provided in Table 1; relevant water-soil behaviour equations and associated parameters are listed in Table 2. Boundary conditions included impervious side walls and free drainage condition at the bottom, whilst variable vertical flow was imposed at the top of the column – a flow-time curve reproducing the hydration sequence developed during the test.

3 Results

3.1 Invasive sensors column (COL-1)

Fig. 7 and Fig. 8 illustrate data corresponding to the COL-1 capacitance and psychrometer sensors, respectively. Pore pressure shows the original psychrometers data record, while EC-5 data have been corrected using the calibration function for granite fines (see Fig. 5). Volumetric water content (θ) was then transformed into degree of saturation (S_w) based on the mean porosity of the bed where the sensor was emplaced. The figures also illustrate the best fit obtained from the numerical modelling of water saturation (Fig. 7) and pore pressure (Fig. 8), at sensor heights. Above the sensor curves, both figures display the water balance of the column. Water contribution steps (WP) are labelled by the theoretical degree of saturation (S_{Tw}) achieved, in terms of mean S_w of the whole column. As previously mentioned, the last hydration step flooded the column and, at this point, the hydraulic conductivity was ~$4 \cdot 10^{-6}$ m s^{-1}.

The capacitance sensors data are highly dependent on the sensor depth, the time lags from hydration events and the degree of saturation of the column. The shallowest sensor (11 cm depth) peaks sharply as a result of hydration up to the fourth step. Onwards, despite more water was being poured into the column, S_w remained constant at a value of ~0.62. At deeper positions, EC-5 sensors show peaks associated with the hydration events, although the peaks are smoother because water progressively spreads into the adjacent pore volume. Likewise, at either position, EC-5 sensors remain approximately constant when S_w is around 0.62, i.e., $\theta > 0.35$.

The maximum water content recorded is still significantly below the full saturation value. This indicates that, in COL-1, the field capacity of GF, which highly depends on the compaction, is nearly the same throughout the entire column. Thus, capacitance sensors located at 11 and 17.5 cm display a steadily increasing trend up to a moisture limit of θ~0.35, while deeper sensors show a transient evolution that overcomes this value before steadiness is attained. Such an effect is also observed in the sensor at 24.5 cm depth after the fifth watering episode and later on in the deepest one. This can be interpreted as a buffering effect related to capillary phenomena along the interface of drainage GF-gravel.

Psychrometer also present sharp variations in the shallower positions (up to 13.5 cm depth), while deeper ones respond to watering with a progressive reduction of pore pressure. However, after the first hydration step, only the sensors located at 27 and 32 cm depth have recorded pore pressure variations; psychrometers at 17.5 and 34.5 cm depth remained unresponsive during the test.

The interpretation of psychrometers data at medium-high soil moisture is inaccurate. Note that, according to the water retention curve for GF reported by

Barrientos et al. (2010), suction lays below 0.05 MPa at $\theta > 0.25$. In as much as this value fits into the lower edge of the sensor response, the recorded values may only be considered representative of the soil moisture only during the first two hydration episodes. That means that we only can take them as qualitative indicators of the transition from a low to a medium moisture domain.

3.2 Numerical modelling

Because of the uncertainty in the data reported by the psychrometers at medium-high moisture contents, only the results obtained by capacitance sensors were considered for numerical modelling. That was conducted to determine the hydraulic conductivity K_0 and the associated moisture conditions, θ_S. The numerical model was addressed using an optimization approach to the measured data, applying equations and controlling the parameters shown in Table 2.

The evolution of the degree of saturation was analysed at 67 discrete times (N), and the relative mean error (M_P) determined from the theoretical (R_t) and the experimental (R_e) observation using the following expression:

$$M_P = \frac{1}{N}\sum_{i=1}^{N}\frac{\left(R_t^i - R_e^i\right)^2}{\left(R_e^i\right)^2} \qquad (2)$$

Applying Eq. 2 to each one of the four capacity probes, a best fit was obtained using a K_0 *value of* $2{\cdot}10^{-6}$ m s^{-1}. That corresponds with a maximum soil moisture of 0.39. For these conditions, M_P was 0.03, 0.04, 0.004 and 0.006, for the capacitance sensors located at 11, 17.5, 24.5 and 32 cm depth, respectively (Fig. 7 and 8). Further uncertainties associated with the accuracy of instrumentation and other random errors were considered in an exploratory sensitivity analysis carried out with respect to K_0, θ_S, and the water retention curve parameters α and m. This analysis showed that the determination of parameter m and also the estimation of θ_s must be carefully addressed because changes of ~5% in any of them might affect the result of the simulation up to 15-20%. The sensitivity analysis is fully presented as supplementary material.

3.3 Non-invasive sensors column (COL-2)

Fig. 9 shows the water balance distribution resulting from COL-2 test. Although the test extended over two weeks, the results presented here focus on the last five days as they better highlight the most relevant features.

Fig. 10 shows the distribution of the water in the column at six different hydration states labelled with the mean degree of saturation (S_{Tw}) estimated from the water balance. The 3D plots illustrate the degree of saturation (S_w) through 160º open-slices on the upper column, where GF were emplaced; the lower part, which was filled with sand, is not represented. In addition, the figure also shows 2D saturation sections at 0.1 (AA'), 0.15 (BB') and 0.2 (CC') m depth. The first stage (S_{Tw}=0.45) is the initial condition of the column, while those following correspond to the S_w distribution at some later time, once watering has occurred.

There is a general agreement between the progressive increase of moisture based on the electrical measurements and those obtained through water balance computation. The moisture distribution is more homogeneous in the upper part of the column (where the degree of saturation is lower), after evert single hydration event. This becomes less significant when moisture content increases (S_{Tw}=0.72 and 0.75), which may be interpreted as resulting from: i) gravity-driven fast flows towards deeper levels; ii) evaporation (~1.74 mm d^{-1}); or iii) a combination of both effects. The last watering step coincided with the first appearance of outflowing of leachates at the bottom of the column. At that moment, the degree of saturation reached a value of ~0.7, which is equivalent to a volumetric water content of ~0.39.

Fig. 10 illustrates preferential pathways located at the sides of the column during the early stages of hydration. In the following watering episodes preferential flow gains importance but, after some time, this effect declines and moisture distribution tends to homogenize in the column. The preferential pathways display an annular distribution that could be related to perturbations induced while assembling the column or during its compaction. Among the possible causes explaining preferential pathways, it is worth highlighting the following: i) grain arching upon compaction; ii) fissuring associated with minor moisture anisotropies; iii) local over compaction resulting from the insertion of electrodes. Regardless of the cause, preferential flow has triggered the formation of gravity-driven high saturation fingers during the earliest watering stages (Glass and Yarrington 1996), an effect that was later progressively attenuated as a result of the advance of the saturation front.

4 Discussion

The experimental results indicate that the field capacity of GF ranges from 0.35 to 0.39, in terms of water content. This range is sensitive to compaction, since the highest value is observed in COL-2, which presented lower porosity than COL-1. However, according to the numerical modelling, the best fit is obtained for a field capacity ~0.39. This difference leads us to conjecture that experimental data from COL-1 might be limited by the resolution of the capacitance sensors at high moistures contents rather than by compaction itself.

Simulated and measured degree of saturation match both qualitatively and quantitatively throughout the studied domain. By contrast, soil suction evolved differently due to uncertainty in the measurements from psychrometers at high moisture contents. Those parameters under unsaturated conditions and relations used for modelling yield reasonable results, exhibiting a realistic retardation of the wetting front moving through the column. In addition, the hydraulic conductivity shown by GF at the yield capacity in COL-1 was $4\cdot10^{-6}$ m s^{-1}, which is consistent with the results of numerical modelling ($2\cdot10^{-6}$ m s^{-1}). This differs by several orders of magnitude from the values reported in Barrientos (2007), which were mainly derived from oedometer tests ($K_s < 10^{-8}$ m s^{-1} or $K_s \sim 6\cdot10^{-7}$ m s^{-1} in the worst case scenario). However, the same author reports an in-situ hydraulic conductivity ~4·10-6 m s^{-1} resulting from a Lefranc-type test conducted in a self-compacted GF landfill which is readily comparable with our assessment, which we consider representative of field service conditions.

In so far as the modelling neglects irregularities in the column, the agreement indicates that the hydrodynamics of the system is not very much affected by the formation of preferential pathways; however, data obtained from COL-2 suggests the contrary, where the generation of gravity fingers related to early stages of hydration is apparent. The origin of gravity fingers is commonly associated with local heterogeneities in the soil matrix. Without considering the role of grain arching in COL-2, driving electrodes into the soil column during assembly might have also contributed to develop local heterogeneity features. On the other hand, electrical data and processed images allow the identification of 3D structures that could be of great interest for larger scale contexts.

The use of capacitance sensors in COL-1 at a larger scale would render a rapid respond to changes in the soil moisture, which contrasts with the fact that capacitance probes are only informative of the small volume of porous media adjacent to the sensor. Moreover, the study also reveals that the use of psychrometers might not be adequate to accurately monitor watering processes in granular, fine grained materials. Even if psychrometers are neglected, a combination of electrical mapping and point moisture determinations based on capacitance probes has a great informative potential when considering larger scale tests.

Whatever the tool used for monitoring moisture changes, a calibration from one soil to another is always required. The methodology used to calibrate the electrical response of granite sawdust has provided valuable information for the interpretation of the experimental data. The standard Proctor test is a fast, cheap and simple way to obtain reasonably homogenous samples for the determination of different physical properties. Therefore, it constitutes a complementary analysis technique when electrical properties are required.

The techniques used in this study have provided useful information regarding the behaviour of GF which were progressively saturated with water starting from low moisture content. The real-time monitoring of the soil response as a result of the hydration-front advance and the test scale, has allowed the recognition of phenomena and structures that single permeability tests would have neglected. Furthermore, the study partially fulfils a knowledge gap regarding the non-saturated hydrodynamics of GF. Since real atmospheric conditions combine wet and dry periods, the information reported in this study is valuable for understanding and predict the hydration of layers of granite fines exposed to long dry periods.

The potential use of granite sawdust as compacted liner or cover layer in landfills widely rests on its hydrodynamic properties and also because it represents a suitable and elegant strategy of sustainable waste management. According to RD 1481/2001 dealing with the landfill of waste (which transposes the 1999/31/EC

Directive to the Spanish law) the landfill base and sides shall consist of a mineral layer which satisfies permeability (K_s) and thickness (T) requirements with a combined effect in terms of protection of soil, groundwater and surface water at least equivalent to the one resulting from the following requirements: i) for hazardous waste $K_s \leq 10^{-9}$ m s^{-1} and $T \geq 5$ m; ii) for non-hazardous waste $K_s \leq 10^{-9}$ m s^{-1} and T > 1 m; iii) for inert waste, $K_s \leq 10^{-7}$ m s^{-1}, $T \geq 1$ m. Therefore, according with our results, the direct application of GF for such a purpose is not directly granted unless greater compaction energy (in excess to the relatively gentle 600 kN-m/m^3 of the standard Proctor conditions used in our study) is applied, as it is expected for this type of engineering elements. Furthermore, our results do not preclude the use of standard Proctor-compacted GF in capillary barrier configurations (e.g., Khire et al. 2000), which would represent a suitable alternative as suggested in Falcon-Suarez (2011).

5 Conclusions

Two large-scale column infiltration tests have been performed to characterize the hydrodynamic properties of standard Proctor-compacted unsaturated granite sawdust. The two columns have been widely instrumented and they have provided useful data to monitor the progressive saturation of GF (and corresponding moisture evolution) and to model the time-dependent behaviour of the overall system. Worth mentioning among the results are the identification of features and structures that occur at the early stages of hydration (e.g., fingering) that, if neglected, could lead to incomplete interpretations. Furthermore, the calibration of the resistivity electrodes based on standard Proctor-compacted specimens provides with a straightforward, technique that can be routinely applied to reconstituted soils of different compositions when performing electrical resistivity surveys.

The hydrodynamic study illustrates that GF have a yield capacity ~0.39 while the corresponding saturated hydraulic conductivity is ~$2\cdot10^{-6}$ m s^{-1}. Both parameters are of the utmost importance when considering water storage and the hydraulic performance of GF either compacted in a single layer or in multilayer systems or capillary barriers. To this respect, based on the present results and mandatory limits of the European and Spanish waste landfill regulation standard Proctor-compacted GF would not be a suitable material for single-layer capping structures. However, enhanced compaction (using, for instance sheepsfoot-type rollers in the field or modified-effort Proctor test, ASTM (2009), in the laboratory) makes possible the attainment of higher material densities and concomitantly lower permeability values. Moreover, improved design considerations using, for instance, multilayer systems or capillary barriers can render GF a useful and cost-effective alternative to the more expensive geomembrane-based solutions.

Acknowledgments

Funds for this work have been provided by the Ministry of Science and Innovation (BIA2005-07916-C02-01), Xunta de Galicia (10REM003CT & 10MDS007CT) and the European Regional Development Funds 2007/2013. Gratefully acknowledged are the Geoevironmental Research Centre at Cardiff University, where the numerical modelling was carried out, and BGR of Hannover, where the experimental procedure was partially undertaken. Support of the Fundación Centro Tecnolóxico do Granito is kindly acknowledged.

References

American Society for Testing and Materials (2007) Standard test methods for laboratory compaction characteristics of soil using standard effort (12 400 ft-lbf/ft (600 kN-m/m)). ASTM Standard D698-07e1. ASTM, West Conshohocken, PA.

American Society for Testing and Materials (2009) Standard test methods for laboratory compaction characteristics of soil using modified effort (56,000 ft-lbf/ft3 (2,700 kN-m/m3)). ASTM Standard D1557. ASTM, West Conshohocken, PA.

Archie GE (1942) The electrical resistivity log as an aid in determining some reservoir characteristics. Trans Am Inst Min Metall Petrol Eng 146: 54-62

Barrientos V, Delgado J, Navarro V, Juncosa R, Falcon I, Vázquez A (2010) Characterization and geochemical-geotechnical properties of granite sawdust produced by the dimension stone industry of O Porrino (Pontevedra, Spain). Q J Eng Geol Hydroge 43: 141-155. doi: 10.1144/1470-9236/08-098

Borghetti A, De Oliveira M, Paulo V, Moreira PS, Claudia M, Gondim RM (2009) Design of a Dry Cover Pilot Test for Acid Mine Drainage Abatement in Southern Brazil I: Materials Characterization and Numerical Modeling. Mine Water Environ 28: 219-231. doi: 10.1007/s10230-009-0077-5

Campbell GS, Campbell CS, Daniel H (2005) Water content and potential, measurement. In: Hillel D. (ed) Encyclopedia of Soils in the Environment, Vol. 4, Oxford, pp 253-257

Carro D, Delgado J, Vázquez A, Barrientos V, Juncosa R (2008) Final Disposal of the Wastes Associated with the Oil Spill of the Tanker Prestige through its

Stabilization with Quicklime and Granite Fines. Soil Sediment Contam 17: 393-410. doi: 10.1080/15320380802146636

Delgado J, Vázquez A, Juncosa R, Barrientos V (2006) Geochemical assessment of the contaminant potential of granite fines produced during sawing and related processes associated to the dimension stone industry. J Geochem Explor 88: 24-27. doi: 10.1016/j.gexplo.2005.08.009

Espinha Marques J, Samper J, Pisani B, Alvares D, Carvalho J, Chaminé H, Marques J, Vieira G, Mora C, Sodré Borges F (2011) Evaluation of water resources in a high-mountain basin in Serra da Estrela, Central Portugal, using a semi-distributed hydrological model. Environ Earth Sci 62: 1219-1234. doi: 10.1007/s12665-010-0610-7

Falcon-Suarez I (2011) Los serrines de granito como barrera de impermeabilización para su uso en vertederos. Dissertation, Universidade da Coruña

Falcon-Suarez I, Rammlmair D, Juncosa-Rivera R, Delgado-Martin J (2014) Application of Rhizon SMS for the Assessment of the Hydrodynamic Properties of Unconsolidated Fine Grained Materials. Eng Geol 172: 69-76. doi: 10.1016/j.enggeo.2014.02.001

Fraser J, McBride RA (2000) The utility of aggregate processing fines in the rehabilitation of dolomite quarries. Land Degrad Dev 11: 1-17. doi: 10.1002/(SICI)1099-145X(200001/02)

Glass RJ, Yarrington L (1996) Simulation of gravity fingering in porous media using a modified invasion percolation model. Geoderma 70: 231-252. doi: 10.1016/0016-7061(95)00087-9

Günther T, Rücker C (2013) Boundless Electrical Resistivity Tomography, BERT – The User Tutorial. Version 2.0. http://resistivity.net/download/bert-tutorialpdf. Accessed 25 October 2007

ICAR (2000) An investigation of the status of by-product fines in the United States. International Center for Aggregate Research Report 101-1, Austin

Kelleners TJ, Soppe RWO, Ayars JE, Skaggs TH (2004a) Calibration of capacitance probe sensors in a saline silty clay soil. Soil Sci Soc Am J 68: 770-778. doi: 10.2136/sssaj2004.7700

Kelleners TJ, Soppe RWO, Robinson DA, Schaap MG, Ayars JE, Skaggs TH (2004b) Calibration of capacitance probe sensors using electric circuit theory. Soil Soil Sci Soc Am J 68: 430-439. doi: 10.2136/sssaj2004.0430

Khire MV, Benson CH, Bosscher PJ (2000) Capillary barriers: Design variables and water balance. J Geotech Geoenv Eng 126: 695-708. doi: 10.1061/(ASCE)1090-0241

Mualem Y (1976) A new model for predicting the hydraulic conductivity of unsaturated porous media. Water Resour Res 12: 513-522. doi: 10.1029/WR012i003p00513

Navarro V, Barrientos V, Yustres A, Delgado J (2008) Settlement of embankment fills constructed of granite fines. Comput Geosci 34: 978-992. doi: 10.1016/j.cageo.2007.07.007

Redwan M, Rammlmair D (2010) Simultaneous monitoring of water saturation and fluid conductivity in unconsolidated sand columns. Soil Science Society of America Journal 74: 1457-1468. doi: 10.2136/sssaj2009.0398

Seidel K, Lange G (2007) Direct Current Resistivity Methods. In: Springer (eds) Environmental Geology, Berlin, pp 205-37. doi: 10.1007/978-3-540-74671-3_8

Seeberg-Elverfeldt J, Schlüter M, Feseker T, Kölling M (2005) A Rhizon in situ sampler (RISS) for pore water sampling from aquatic sediments. Limnol Oceanogr Meth 3: 361-371. doi: 10.4319/lom.2005.3.361

Shackelford CD, Javed F (1991) Large-scale laboratory permeability testing of a compacted clay soil. Geotech Test J 14: 171-179. doi: 10.1520/GTJ10559J

Terzaghi K, Peck RB, Mesri G (1996) Soil Mechanics In Engineering Practice, 3rd edn. Wiley-Interscience, New York

Thomas HR, He Y (1997) A coupled heat–moisture transfer theory for deformable unsaturated soil and its algorithmic implementation. Int J Numer Methods Eng 40: 3421-3441. doi: 10.1002/(SICI)1097-0207(19970930)

Thomas HR, He Y (1998) Modelling the behaviour of unsaturated soil using an elastoplastic constitutive model. Geotechnique 48: 589-603. doi: 10.1680/geot.1998.48.5.589

Thomas H, Sedighi M, Vardon P (2012) Diffusive Reactive Transport of Multicomponent Chemicals Under Coupled Thermal, Hydraulic, Chemical and Mechanical Conditions. Geotech Geol Eng 30: 841-857. doi: 10.1007/s10706-012-9502-9

Topp GC, Davis JL, Annan AP (1980) Electromagnetic determination of soil water content: measurement in coaxial transmission lines. Water Resour Res 16: 574-582. doi: 10.1029/WR016i003p00574

Van Genuchten MT (1980) A closed-form equation for predicting the hydraulic conductivity of soil. Soil Sci Soc Am J 44: 892-898. doi:10.2136/sssaj1980.03615995004400050002x

Vázquez A (2005) Modelización Geoquímica de los Serrines de Granito. Dissertation, Universidade da Coruña

Vázquez A, Juncosa R, Barrientos V, Falcon I, Delgado J, Navarro V (2007) Hydrodynamic and reactive transport modeling of the behavior of compacted granite saw dust for landfill liners and covers. In: Bullen TD and Y Wand Y (eds) Water-Rock Interaction Vol. 1, Rotterdam, pp 653-657

Table 1 Initial conditions of column tests

	Top	Bottom	ρ_d	ϕ	θ	S_w	Sensors	
	(cm)		(g cm^{-3})	(cm^3 cm^{-3})	(cm^3 cm^{-3})			
COL-1								
	38.5		1.26	0.61	0.18	0.29		
	34		1.27	0.6	0.17	0.29	*Psy*	
	29		1.23	0.61	0.13	0.21	*Psy*	*EC*
	25		1.25	0.61	0.19	0.3	*Psy*	
	20		1.16	0.64	0.17	0.27	*Psy*	*EC*
	15.5		1.21	0.62	0.17	0.28	*Psy*	*EC*
	10.5		1.2	0.62	0.17	0.28	*Psy*	*EC*
	4		1.11	0.65	0.17	0.25	*Psy*	
COL-2								
	46		1.37	0.57	0.26	0.46		
	32		1.37	0.57	0.27	0.47		
	22		1.3	0.59	0.26	0.44		
	8		1.44	0.55	0.28	0.51		

Top and bottom position of each layer from the top of the column; ρ_d, dry density; ϕ, porosity; θ, moisture; S_w, degree of saturation; Psy and EC are psychrometers (PCT-55-15-SF) and EC-5 soil moisture sensors, at their respective locations.

Table 2 Hydraulic model parameters and equations

Parameters	Expression*	Value	Unit	Reference
Specific degree of saturation (S_e)	$S_e = \frac{\theta_i - \theta_r}{\theta_s - \theta_r}$	--	--	Experimental
Suction (ψ_i)	$\psi_i = \frac{\left(S_e^m - 1\right)^{1/n}}{-\alpha}$	--	kPa	Van Genuchten (1980)
Hydraulic conductivity (k_i)	$k(\psi_i) = K_0 S_e^{0.5}\left(1-\left(1-S_e^{1/m}\right)^m\right)^2$	--	$m\ s^{-1}$	(Mualem, 1976)
Granite fines parameters (water retention curve)	α	0.193	kPa^{-1}	Barrientos et al. (2010)
	m	0.291	--	Barrientos et al. (2010)
	n	1.41	--	Barrientos et al. (2010)
	θ_r	0.09	$m^3\ m^{-3}$	Barrientos et al. (2010)

*Subscript i, initial conditions from experimental data; θ, volumetric water content (r, residual; s, saturated); ϕ, porosity; K_0, hydraulic conductivity at maximum saturation conditions

Fig. 1 Dimension stone activities in Pontevedra (Spain): **a**, panoramic view of the quarries; **b**, primary block; **c**, workshops; **d**, granite saw dust.

Fig. 2 Experimental column COL-1: **a,** global view of the column; **b,** column schematic where elements are numbered with [1] acrylic column, [2] granite fines layers, [3] psychrometers, [4] EC-5 soil moisture sensors, [5] gravel layer, [6] spacer-annulus, [7, 8] lateral and central drainage.

Fig. 3 Experimental column, COL-2. **a**, global view of the column: [1] SIPLab connectors, [2] PVC column, [3] Electrodes, [4] electrodes to SIPLab-connectors cables, [5] drainage system. **b**, transversal (top) and longitudinal (bottom) drawing of the electrode distribution and the mesh generated by software BERT.

Fig. 4 Experimental setup to measure the bulk electrical conductivity of Standard Proctor samples: [1] electrodes; [2] acrylic mould where the sample is emplaced; [3] SIPLab equipment.

Fig. 5 Calibration of the moisture signal recorded by EC-5 sensors on granite fines using Standard Proctor samples. θ_P and θ_E are moistures determined from Proctor properties and measured by EC-5 sensors, respectively.

Fig. 6 Calibration of the bulk electrical conductivity on GF using Standard Proctor samples at different degrees of saturation. The inner graph compares the bulk electrical conductivity measured ($\sigma_{b,Proctor}$) and calculated according to the Archie's adjustment for GF ($\sigma_{b,Archie}$).

Fig. 7 COL-1 test. Evolution of water content (θ) and degree of saturation (S_w). Results of the numerical modelling are also displayed, in terms of S_w at sensors depths. The water balance (WB) indicates water coming in and out the column ($\pm\Delta w$): L-L and L-C, lateral and central leachates; E, evaporation; WP, water contributions; S_{Tw}, mean degree of saturation calculated at WP instants.

Fig. 8 COL-1 test. Evolution of pore pressure (ψ, suction). Results of the numerical modelling are also displayed, in terms of ψ at sensors depths. The water balance (WB) indicates water coming in and out the column ($\pm\Delta w$): L-L and L-C, lateral and central leachates; E, evaporation; WP, water contributions; S_{Tw}, mean degree of saturation calculated at WP instants.

Fig. 9 Water balance (WB) of COL-2 test: Δw, water coming in (+) and out (-) the column; L-L and L-C, lateral and central leachates; E, evaporation. Dark area involves the steps shown in Figure 11.

Fig. 10 COL-2 test. Evolution of the degree of saturation (Sw) in 3D (top) and 2D sections at 10 (AA'), 15 (BB') and 20 (CC') cm depth. STw, mean degree of saturation of the column obtained from the water balance.

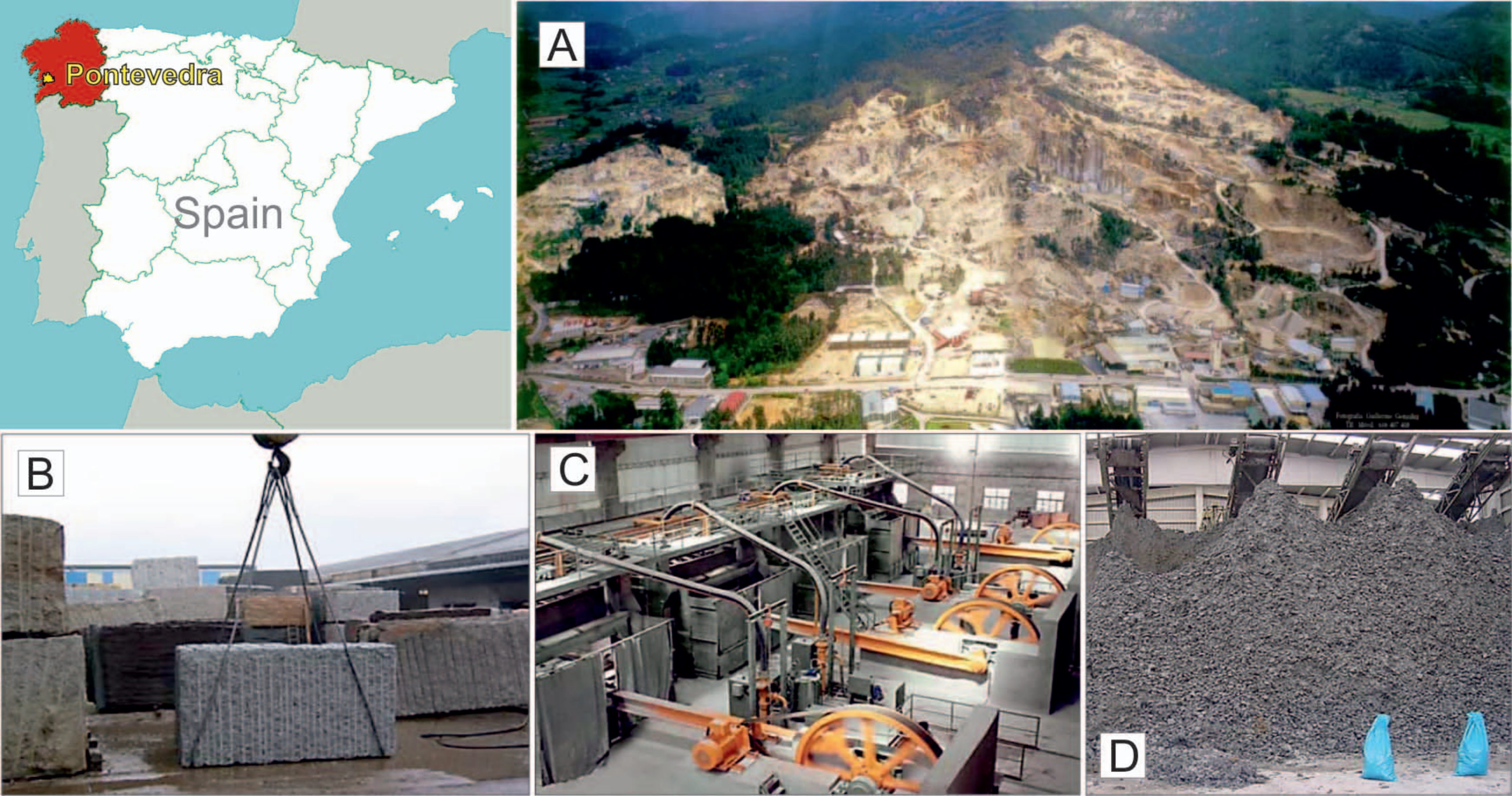
Pontevedra
Spain
A
B
C
D

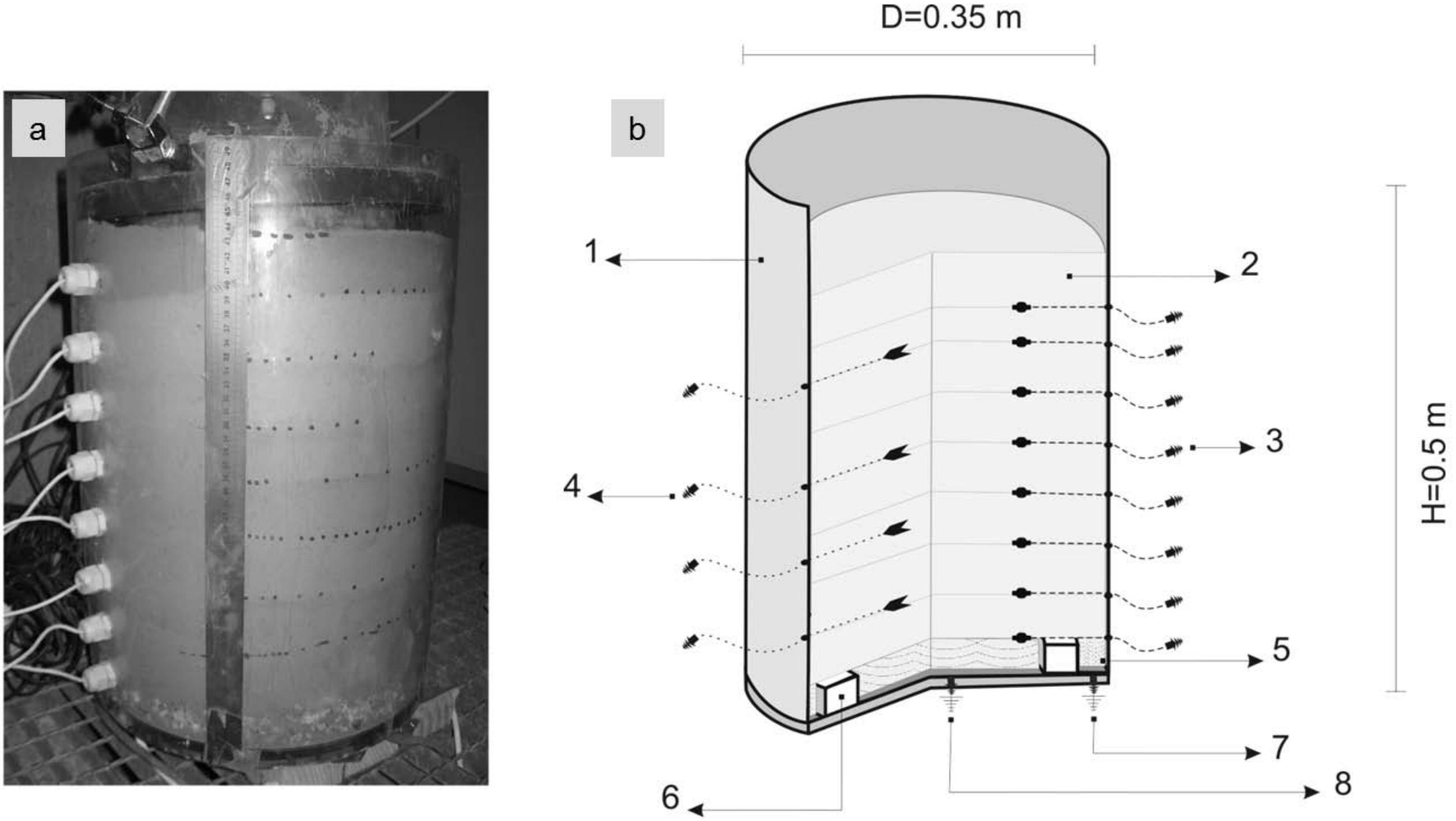
a
b
D=0.35 m
H=0.5 m
1
2
3
4
5
6
7
8

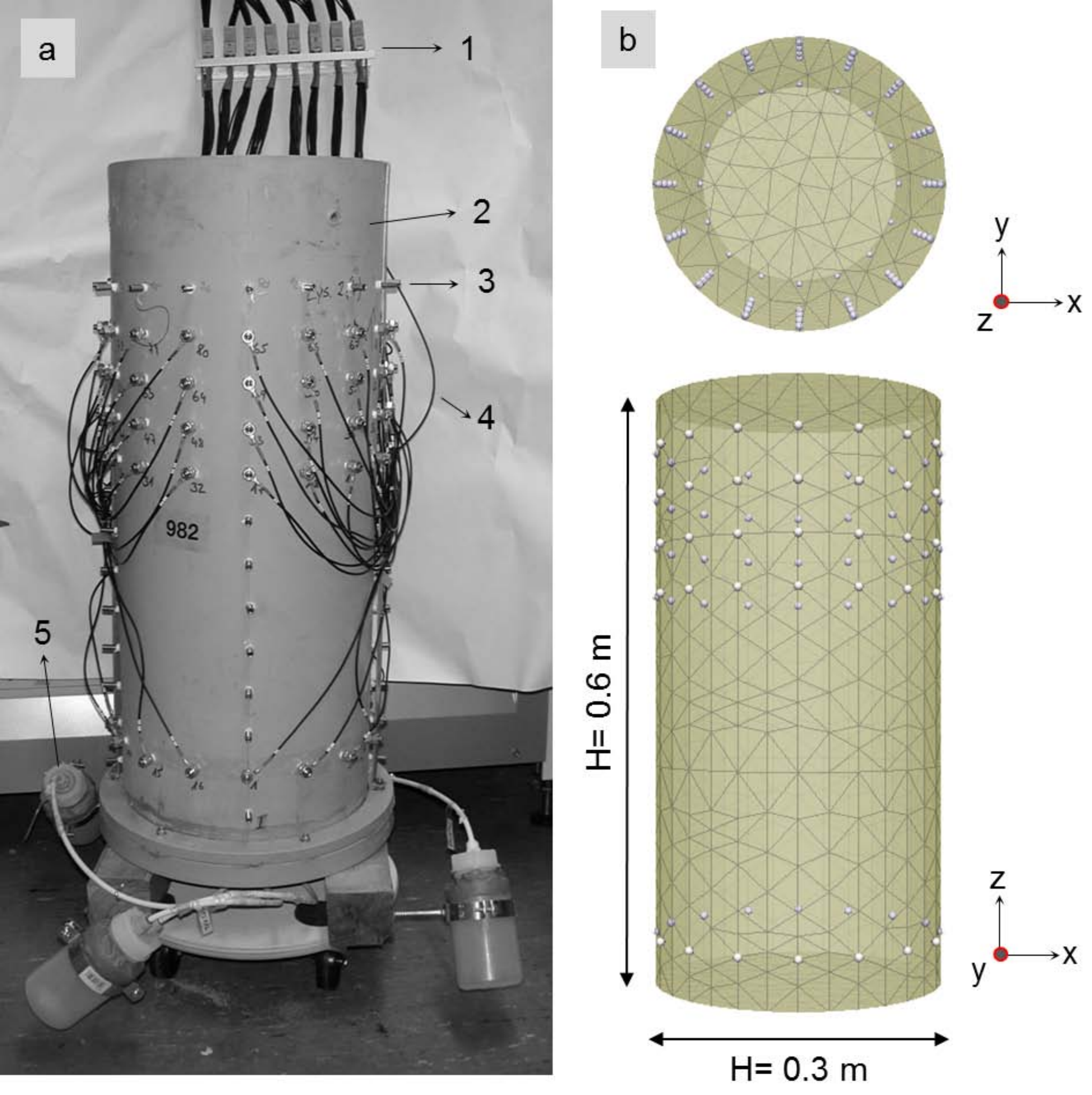
a
1
2
3
4
5
982
b
y
x
z
H= 0.6 m
H= 0.3 m
z
x
y

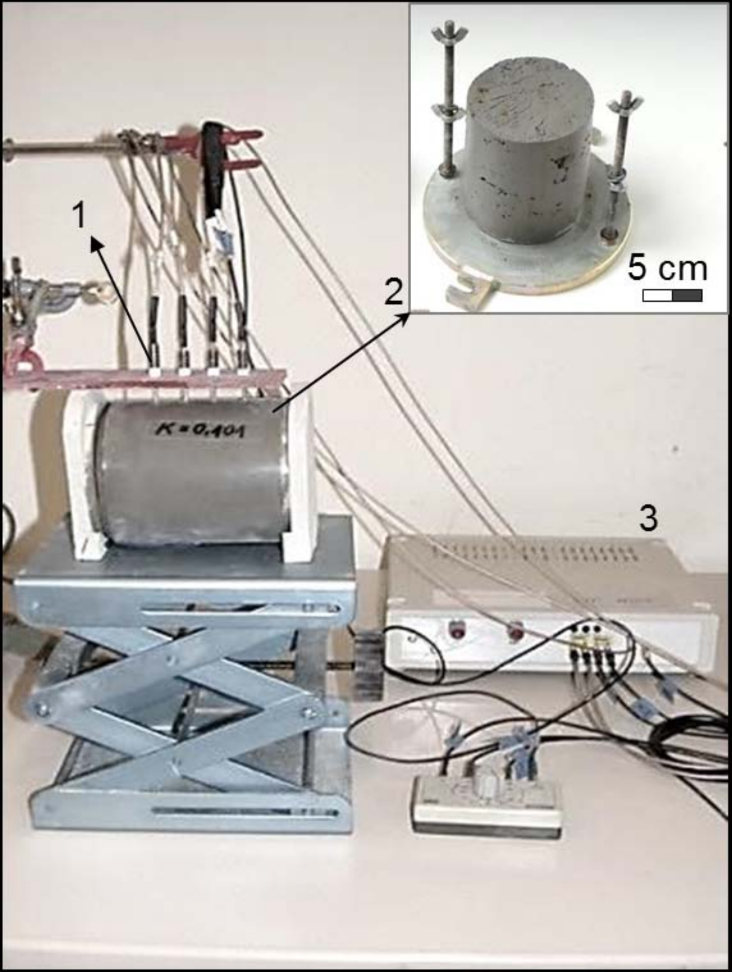
1
2
3
K = 0,401
5 cm

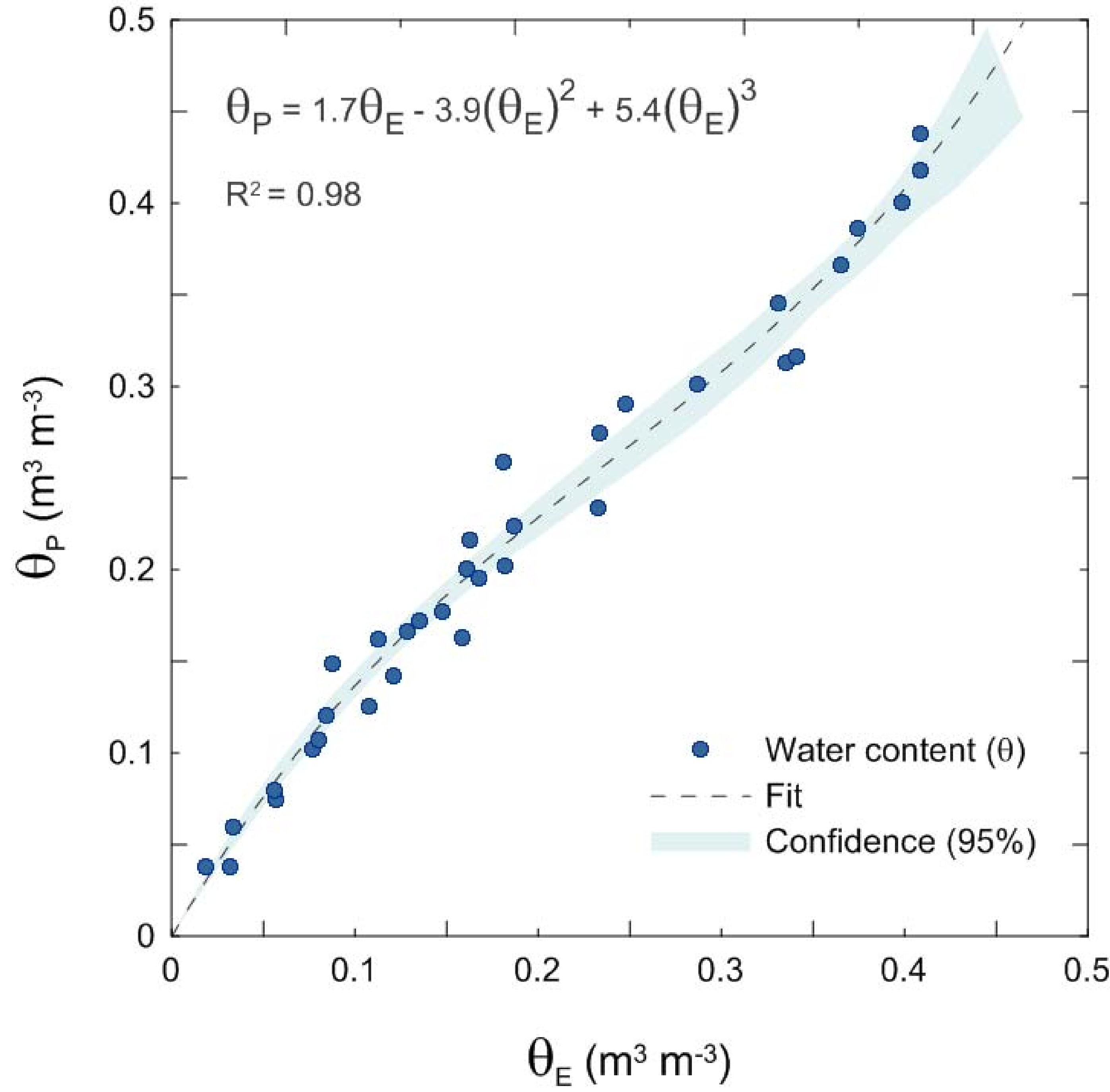
$\theta_P = 1.7\theta_E - 3.9(\theta_E)^2 + 5.4(\theta_E)^3$
$R^2 = 0.98$
● Water content (θ)
Fit
Confidence (95%)
θ_P (m^3 m^{-3})
θ_E (m^3 m^{-3})
0
0.1
0.2
0.3
0.4
0.5
0
0.1
0.2
0.3
0.4
0.5

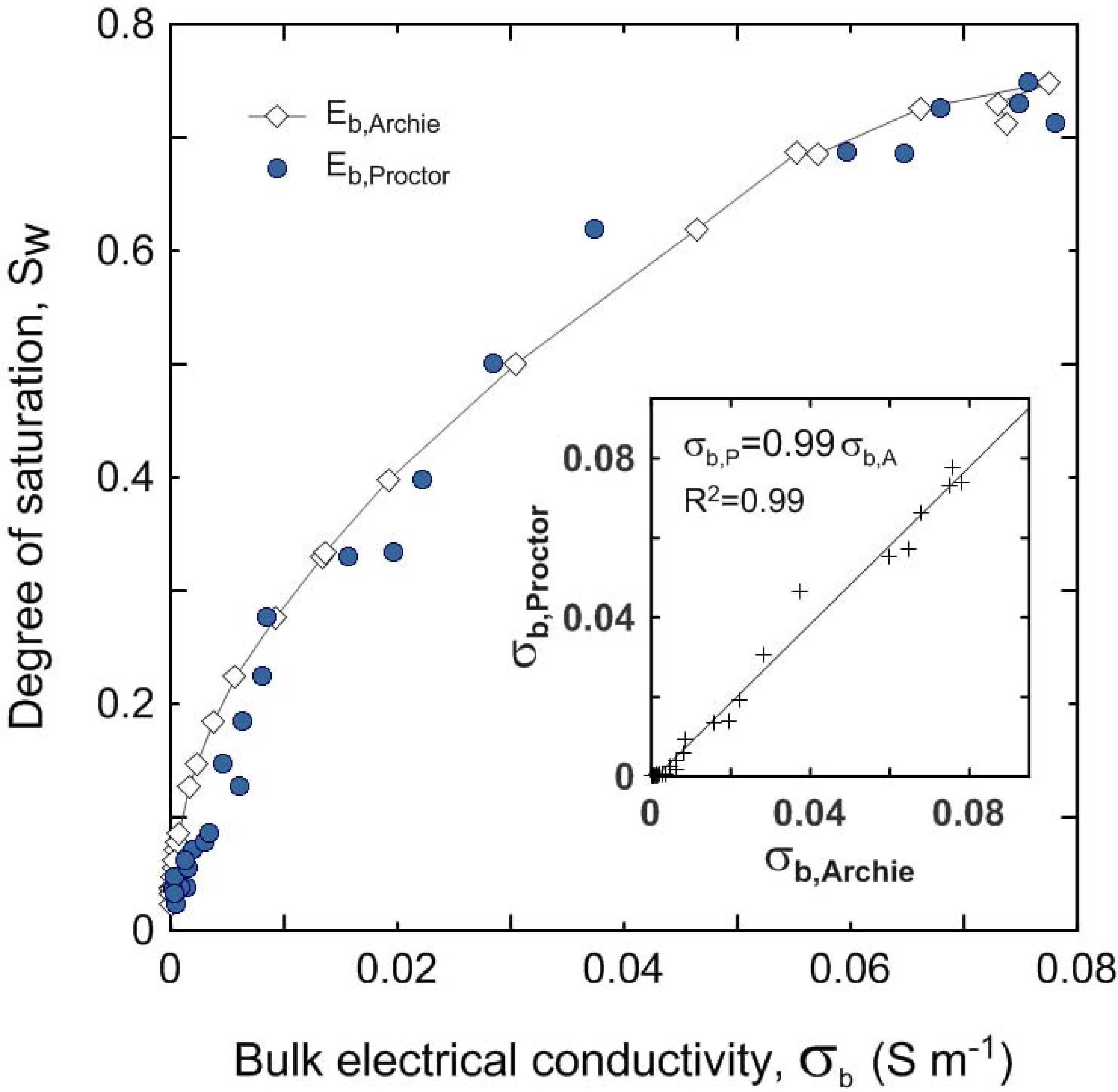
0.8
0.6
0.4
0.2
0
Degree of saturation, Sw
0
0.02
0.04
0.06
0.08
Bulk electrical conductivity, σb (S m-1)
Eb,Archie
Eb,Proctor
σb,P=0.99 σb,A
R2=0.99
0.08
0.04
0
σb,Proctor
0
0.04
0.08
σb,Archie

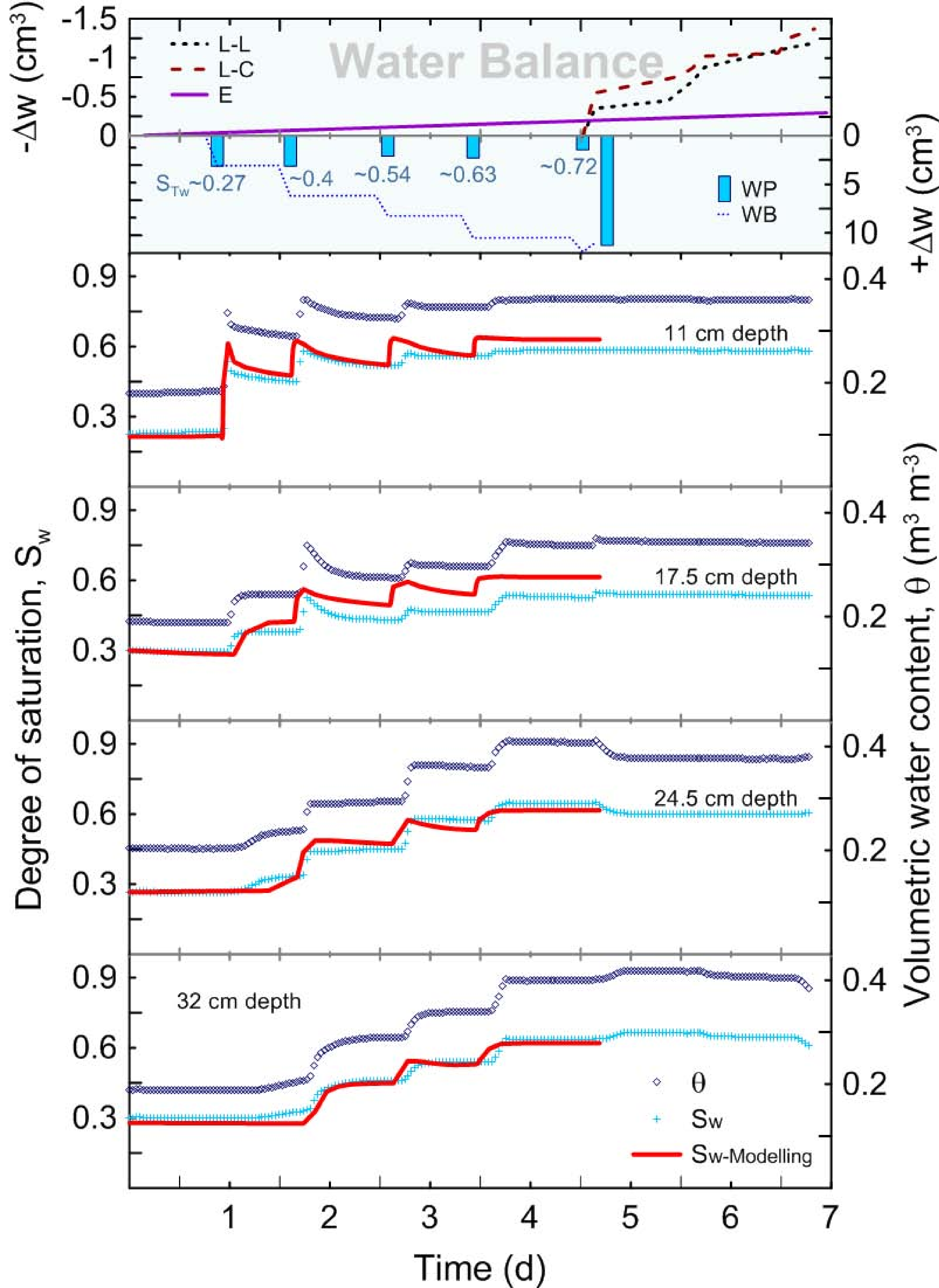
Water Balance
L-L
L-C
E
WP
WB
$-\Delta w$ (cm^3)
$+\Delta w$ (cm^3)
-1.5
-1
-0.5
0
5
10
S_{Tw}~0.27
~0.4
~0.54
~0.63
~0.72
11 cm depth
17.5 cm depth
24.5 cm depth
32 cm depth
0.9
0.6
0.3
0.4
0.2
θ
Sw
Sw-Modelling
Degree of saturation, S_w
Volumetric water content, θ (m^3 m^{-3})
1
2
3
4
5
6
7
Time (d)

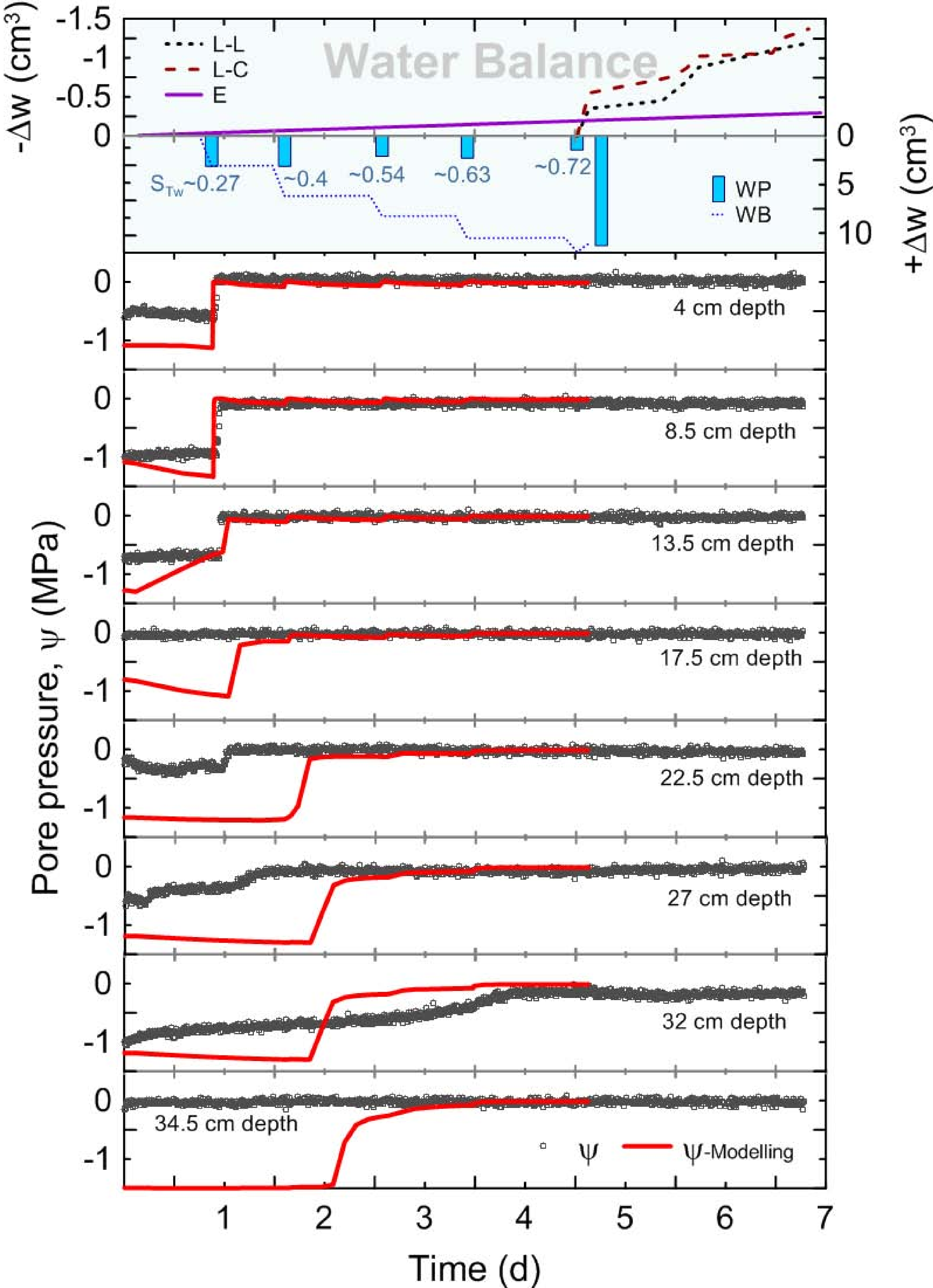
Water Balance
-Δw (cm³)
-1.5
-1
-0.5
0
L-L
L-C
E
S_Tw~0.27
~0.4
~0.54
~0.63
~0.72
WP
WB
+Δw (cm³)
0
5
10
Pore pressure, ψ (MPa)
0
-1
4 cm depth
8.5 cm depth
13.5 cm depth
17.5 cm depth
22.5 cm depth
27 cm depth
32 cm depth
34.5 cm depth
ψ
ψ-Modelling
1
2
3
4
5
6
7
Time (d)

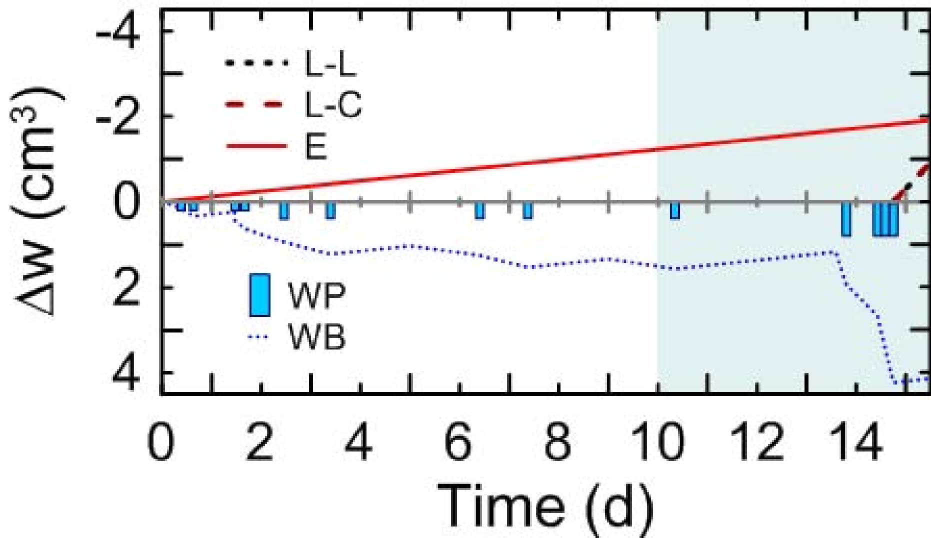
L-L
L-C
E
WP
WB
Δw (cm³)
-4
-2
0
2
4
0
2
4
6
8
10
12
14
Time (d)

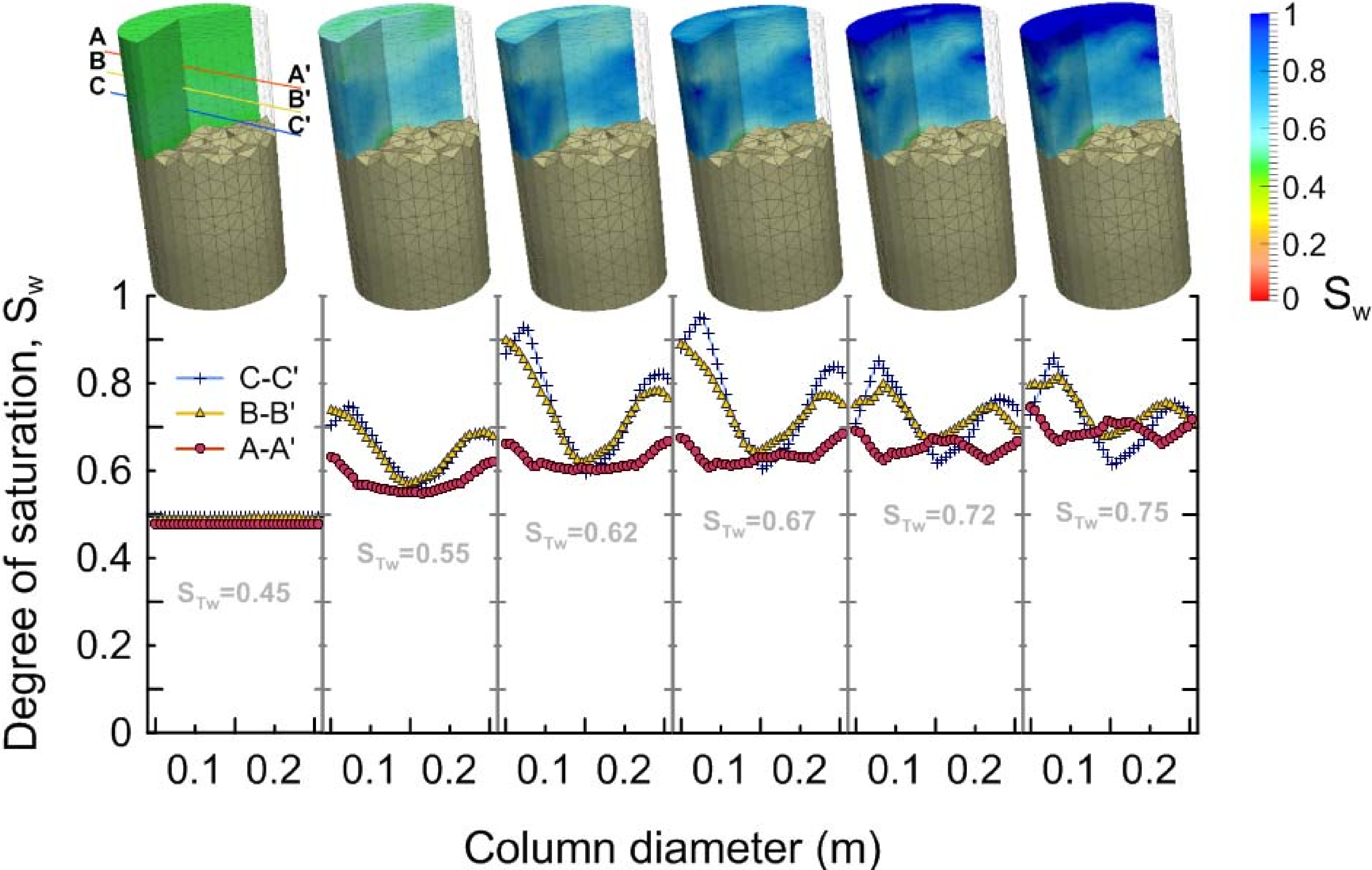
A
B
C
A'
B'
C'
1
0.8
0.6
0.4
0.2
0
S_w
Degree of saturation, S_w
1
0.8
0.6
0.4
0.2
0
C-C'
B-B'
A-A'
S_Tw=0.45
S_Tw=0.55
S_Tw=0.62
S_Tw=0.67
S_Tw=0.72
S_Tw=0.75
0.1
0.2
0.1
0.2
0.1
0.2
0.1
0.2
0.1
0.2
0.1
0.2
Column diameter (m)